



Effect of modified CeO₂ on the performance of PdCu/Ce_{1-x}Ti_xO₂ catalyst for methanol purification

Zhangjie Li¹ · Yongdong Chen¹ · Jie Deng¹ · Li Luo¹ · Wenxiang Gao¹ · Liang Yuan¹

Received: 20 February 2022 / Accepted: 26 April 2022 / Published online: 28 May 2022
© The Author(s), under exclusive licence to Springer-Verlag GmbH Germany, part of Springer Nature 2022

Abstract

In this paper, we prepared a series of Ce_{1-x}Ti_xO₂ ($x=0-0.20$) nanorods by hydrothermal method, which were used to construct the PdCu/Ce_{1-x}Ti_xO₂ catalysts. The Ce_{1-x}Ti_xO₂ and PdCu/Ce_{1-x}Ti_xO₂ samples were characterized by transmission electron microscope (TEM), X-ray photoelectron spectroscopy (XPS), N₂ adsorption–desorption, X-ray diffraction (XRD), inductively coupled plasma optical emission spectrometer (ICP-OES), etc. Catalytic activity, stability, and repeatability of the catalysts for methanol oxidation were investigated. The results show that doping a proper amount of titanium could strengthen the interaction between Ce_{1-x}Ti_xO₂ support and PdCu nanoalloy, thus increasing the oxygen vacancy concentration and promoting Pd species with a higher oxidation state. These modified properties are beneficial for the deep oxidation of methanol. The light-off temperature (T_{50}) and full-conversion temperature (T_{90}) of methanol over the PdCu/CeO₂ catalyst are 108 °C and 159 °C, respectively. The greatest activity improvement is found for PdCu/Ce_{0.9}Ti_{0.1}O₂, which shows the lowest T_{50} of 88 °C and T_{90} of 138 °C. Furthermore, neither PdCu/CeO₂ nor the modified PdCu/CeO₂ catalyst produces by-products and exhibit excellent stability and repeatability throughout the whole test period. This study provides a reference for in-depth understanding and designing of efficient and stable CeO₂-based oxidation catalysts.

Keywords Ceria-based catalysts · Titanium doping · Methanol purification · Oxygen vacancy · Fixed bed · Monolithic catalyst

Introduction

Methanol has the advantage of high-octane value, large latent heat of vaporization and sustainability, so it is the best alternative to fossil fuels (Arnason & Sigfússon 1999; Su et al 2020; Zhen et al 2017). As a new generation of alternative fuel of gasoline vehicle, it can significantly reduce the emission of hydrocarbon compounds (HCs), CO, NO_x and particulate matters. Therefore, it has received widespread attention and has been widely used in developed countries, such as the USA, Japan and Germany. However, the use of methanol as fuel has met resistance owing to the fact that it can produce considerable amount of unburned methanol

especially during the cold start and idling condition (Tang et al 2020; Wang et al 2021a, b; Li and Wey 2021). Recently, Chongqing Vehicle Inspection and Research Institute conducts emission tests on heavy-duty methanol engines (Li et al. 2021). The results show that the content of methanol in the exhaust gas during cold start exhibits a high value of 10–30 µg/mL. It is known that methanol and its metabolite, like formaldehyde and formic acid, are harmful for the nervous and blood systems of humans (Aakko-Saksa et al. 2020; Zhang et al. 2020). Therefore, developing an efficient catalyst for complete methanol oxidation at low temperature is of great significance.

In recent decades, a large number of supported catalysts, especially these based on precious metals (such as Pd (Chen et al. 2019a, b; Luo et al. 2015; Luo et al. 2012), Pt (Hao et al. 2021; Tian et al. 2021; Tian et al. 2017), Ag (Satra et al. 2020; Kumar et al. 2018), etc.) have been developed for complete oxidation of methanol. Among these catalysts, the supported Pd catalyst often has better catalytic activity, but the high cost limits its wide application. Studies have shown that combining Pd and Cu into a nanoalloy can not only reduce

Responsible editor George Z. Kyzas.

✉ Yongdong Chen
yongdongchen@swpu.edu.cn

¹ College of Chemistry and Chemical Engineering, Southwest Petroleum University, Chengdu 610500, People's Republic of China

the amount of Pd, but also produce better catalytic performance (Chen et al. 2018; Gholinejad et al. 2021; Guo et al. 2019). However, the high gas hourly space velocity (GHSV) of vehicle exhaust and low temperature during cold start still make the complete oxidation of methanol a huge challenge.

With respect to the support material in the supported catalyst, ceria (Chen et al. 2017; Grieshammer 2017; Hao et al. 2021; Wang et al. 2021a, b; Shan et al. 2020; Cui et al. 2020) (CeO_2) has received significant attention, because of its unique oxygen release/storage capacity and excellent thermal stability. Previous studies have shown that CeO_2 as a support material can not only provide abundant reactive O, but also promote the stable dispersion of precious metals, consequently accelerates catalytic performance. Therefore, CeO_2 -based materials are currently the most important catalytic materials used in automotive exhaust purification catalysts. Chen and Zheng et al. (Chen et al. 2019a, b) prepared a series of PdCu nanoparticles with different sizes and loaded PdCu nanoparticles on CeO_2 nanorods. They found that the interaction between PdCu and CeO_2 nanorods could promote the catalytic activity for methanol oxidation. However, pure CeO_2 will be severely deactivated overtime, thereby damaging catalytic activity. Doping other metallic cations into ceria lattices is usually an effective method to improve the stability as well as the oxygen storage capacity. TiO_2 (Antonia et al. 2020; Manzorro et al. 2019; Wu and Xing 2020; Zhang et al. 2016) is an attractive catalytic material with high chemical stability, low price and non-toxicity, which has been successfully used in the photocatalytic field. This inspires the design of TiO_2 -modified CeO_2 . Studies have shown that TiO_2 -modified CeO_2 has attracted widespread attention in the field of catalysis because of its ability to enhance the performance of CeO_2 -based materials. Chen et al. (Chen et al. 2019a, b) prepared a spherical $\text{Ce}_{1-x}\text{Ti}_x\text{O}_2$ solid solution catalyst via a co-precipitation method. The results showed that doping titanium ions promotes the generation of more oxygen vacancies, thereby greatly improving the catalytic performance. Considering the modified properties of $\text{Ce}_{1-x}\text{Ti}_x\text{O}_2$ by doping titanium, it is worth to investigate the interaction between PdCu and $\text{Ce}_{1-x}\text{Ti}_x\text{O}_2$, together with its influence on the catalytic performance for complete methanol oxidation.

Therefore, in this work, we firstly prepared monodisperse PdCu nanoparticles by two-step reduction in an ethylene glycol system. Then, we synthesized a series of CeO_2 modified with different contents of titanium via a hydrothermal method and the corresponding supported PdCu/ $\text{Ce}_{1-x}\text{Ti}_x\text{O}_2$ catalysts. To investigate the influence of doping titanium on the properties of $\text{Ce}_{1-x}\text{Ti}_x\text{O}_2$ and PdCu/ $\text{Ce}_{1-x}\text{Ti}_x\text{O}_2$, we characterized the samples from a structural and textural point of view with techniques such as X-ray diffraction (XRD), N_2 adsorption–desorption, and X-ray photoelectron spectroscopy (XPS). Also, the catalytic performances of PdCu/

$\text{Ce}_{1-x}\text{Ti}_x\text{O}_2$ ($x=0-0.20$) catalysts were tested for deep oxidation of methanol. This work focuses on the possible reasons for improved catalytic activity of the deep oxidation of methanol induced by the introduction of titanium.

Experimental

Chemicals

Sodium tetrachloropalladate(II) (Na_2PdCl_4 , 98%, Macklin), copper(II) chloride dihydrate ($\text{CuCl}_2\cdot\text{H}_2\text{O}$, 99.99%, Aladdin), oleylamine (OAm, 80–90%, Aladdin), cerium nitrate ($\text{Ce}(\text{NO}_3)_3\cdot 6\text{H}_2\text{O}$, 99.0–100.0%, AR, Aladdin), titanium sulfate ($\text{Ti}(\text{SO}_4)_2$, 99.9%, AR, Aladdin) and sodium hydroxide (NaOH , $\geq 98.0\%$, AR, Kelong), ethanol ($\text{C}_2\text{H}_5\text{OH}$, 99.7%, AR, Kelong), ethylene glycol ($\text{C}_2\text{H}_6\text{O}_2$, $\geq 99.5\%$, AR, Aladdin), and cyclohexane (C_6H_{12} , $\geq 99.7\%$, AR, Kelong).

Synthesis of PdCu nanoparticles

In the preparation of monodisperse PdCu nanoparticles, $\text{C}_2\text{H}_6\text{O}_2$ was used as reducing agent and solvent. Oleylamine (OAm) and cyclohexane were used as surfactant and extractant, respectively. Typically, Na_2PdCl_4 (0.0375 mmol) and $\text{CuCl}_2\cdot 2\text{H}_2\text{O}$ (0.0125 mmol) were added to a 250 mL three-necked flask containing 100 mL of $\text{C}_2\text{H}_6\text{O}_2$, then 1 mL of OAm was added under mechanical stirring. The sample was first heated to 120 °C for 20 min, then the temperature was increased to 200 °C and kept for 2 h. After cooling down to room temperature, a mixture of $\text{C}_2\text{H}_5\text{OH}$ (100 mL) and cyclohexane (100 mL) was added for extracting PdCu colloidal solution. Then the PdCu colloidal solution was washed with a certain amount of acetone (CH_3COCH_3), centrifuged, and finally the active PdCu nanoparticles were dispersed in cyclohexane. The Pd nanoparticles and Cu nanoparticles are prepared as the same procedure where only Na_2PdCl_4 (0.05 mmol) and only $\text{CuCl}_2\cdot 2\text{H}_2\text{O}$ (0.05 mmol) was used, respectively.

Synthesis of $\text{Ce}_{1-x}\text{Ti}_x\text{O}_2$ nanorods

The $\text{Ce}_{1-x}\text{Ti}_x\text{O}_2$ ($x=0-0.20$) nanorods were prepared by hydrothermal synthesis method. Take the synthesis of $\text{Ce}_{0.95}\text{Ti}_{0.05}\text{O}_2$ as an example. Typically, $\text{Ce}(\text{NO}_3)_3\cdot 6\text{H}_2\text{O}$ (12 mmol), $\text{Ti}(\text{SO}_4)_2$ (0.632 mmol) and excessive NaOH were completely dissolved and mixed together, then the slurry was poured into a 100 mL autoclave and maintained at 100 °C for 20 h. The precipitate was collected by centrifugation and washed thoroughly with deionized water until the supernatant was neutral. The resulting product was dried at 80 °C overnight and then calcined in a muffle furnace at 400 °C for 4 h to obtain $\text{Ce}_{0.95}\text{Ti}_{0.05}\text{O}_2$ powder. The same

synthesis process was applied to synthesize the other materials with different titanium content.

Synthesis of PdCu/Ce_{1-x}Ti_xO₂ catalysts

PdCu nanoparticles on the Ce_{1-x}Ti_xO₂ ($x=0-0.20$) support as the catalysts were synthesized by mechanical co-assembly method. 1 wt% of bimetallic PdCu loading was maintained on the Ce_{1-x}Ti_xO₂ ($x=0-0.20$) support for the catalysts. For instance, to prepare PdCu/Ce_{0.95}Ti_{0.05}O₂ catalyst, the synthesized Ce_{0.95}Ti_{0.05}O₂ powder was dispersed in cyclohexane containing PdCu nanoparticles. After ultrasonic for 30 min, the mixture was mechanically stirred for 24 h at the room temperature. The product was collected by filtering, drying at 50 °C and 0.07 MPa for 12 h, and finally calcining in a muffle furnace at 400 °C for 4 h. The PdCu/Ce_{1-x}Ti_xO₂ catalyst preparation flow scheme is described in Scheme 1.

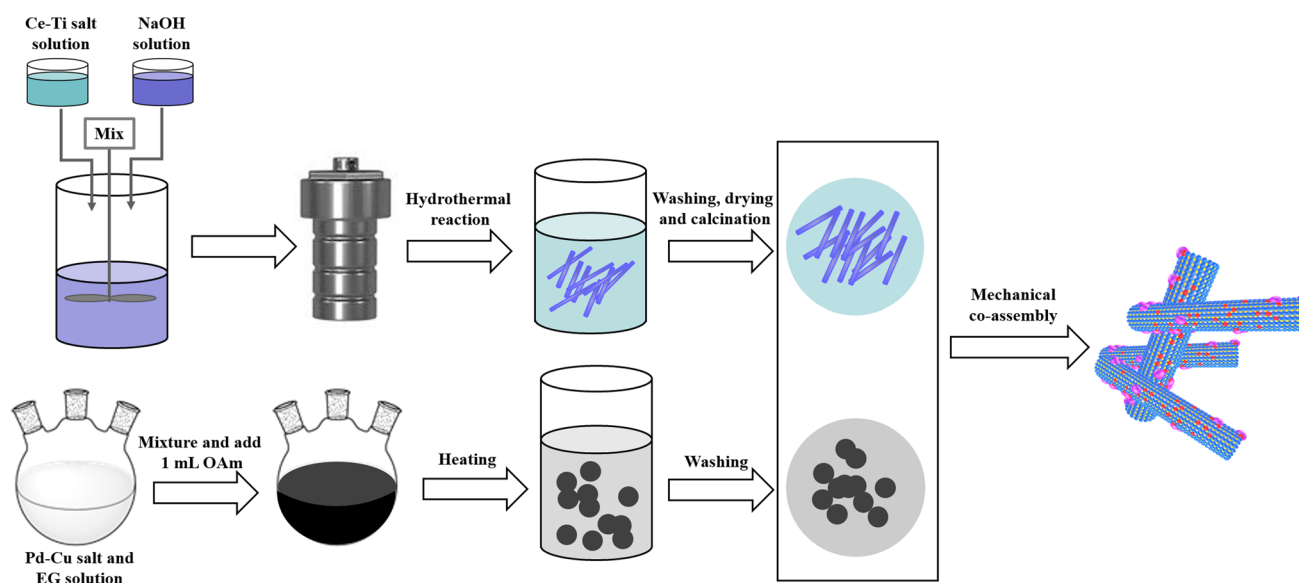
Preparation of PdCu/Ce_{1-x}Ti_xO₂ monolith catalyst

Firstly, the as-obtained PdCu/Ce_{1-x}Ti_xO₂ powder was ball milled with appropriate amount of deionized water to prepare a slurry. Then, the slurry was coated on the cordierite honeycomb ceramic substrate (64 cell·cm⁻², $\Phi=10$ mm, $L=25$ mm). The excess slurry was removed from the monolith channels by the blower and coated repeatedly until approximately 0.35 g slurry was coated on the honeycomb cordierite. The slurry quality was ensured by an electronic

balance. Ultimately, the monolith catalyst was dried at 80 °C overnight and calcined at 400 °C for 4 h.

Characterization techniques

The metal content of the PdCu/Ce_{1-x}Ti_xO₂ catalyst was determined by using an inductively coupled plasma optical emission spectrometry (ICP-OES) (Agilent Technologies, USA). The size and morphology of the sample were observed by transmission electron microscopy (TEM) (FEI, USA) using a Tecnai G² F20 S-TWIN apparatus operated at an accelerating voltage of 200 kV. X-ray powder diffraction (XRD) (Thermo Scientific, USA) was conducted on a DX-1000 CSCX diffractometer using Cu K α radiation operated at 40 kV and 25 mA. The 2θ of the wide angle ranged from 20° to 80° with a scan rate of 0.48°/min. N₂ adsorption–desorption isotherms were recorded at -196 °C using an ASAP 2010 instrument (Micromeritics, USA). Before the measurement, the sample was degassed at 300 °C for 3 h. The specific surface areas were calculated from the adsorption results using the multipoint Brunauer–Emmett–Teller (BET) (Anton Paar, Austria) analysis of the N₂ adsorption isotherms. X-ray photoelectron spectroscopy (XPS) (Thermo Scientific, USA) was performed on a K-Alpha electron spectrometer using a monochromatic Al K α excitation source ($h\nu=1486.6$ eV). The analysis was done at room temperature and a pressure of 6.67×10^{-7} Pa. The C 1s (284.6 eV) of the surface pollution carbon was used to calibrate all the spectra. The peak fitting was completed using XPS PEAK 41 software.



Scheme 1 Schematic illustration of the synthesis process of the PdCu/Ce_{1-x}Ti_xO₂ catalyst, including the preparation of PdCu nanoparticles, Ce_{1-x}Ti_xO₂ nanorods and the final PdCu/Ce_{1-x}Ti_xO₂ catalyst production

Catalytic evaluation

A continuous-flow atmospheric fixed-bed reactor was used to evaluate the methanol complete oxidation reaction activity. The monolithic catalyst was installed in the reaction tube. The reaction gas was composed of the following three parts: 0.02 vol% methanol, 2.0 vol% O₂, and N₂ as the balance gas. The total flow rate was 1015.625 mL·min⁻¹, corresponding to a gas hourly space velocity (GHSV) of 30,000 h⁻¹. The composition of the product was analyzed by Agilent GC7890B gas chromatograph with flame ionization detector (FID) and thermal conductivity detector (TCD). The CH₃OH conversion (conv.) was calculated as follows: conv. % = [(C_{in} - C_{out}) ÷ C_{in}] × 100. Where C_{in} and C_{out} represent the content of methanol in the inlet and outlet gases, respectively.

$$\text{conv. \%} = [(C_{in} - C_{out}) \div C_{in}] \times 100$$

Results and discussions

Characterization of the catalysts

Morphological studies of samples

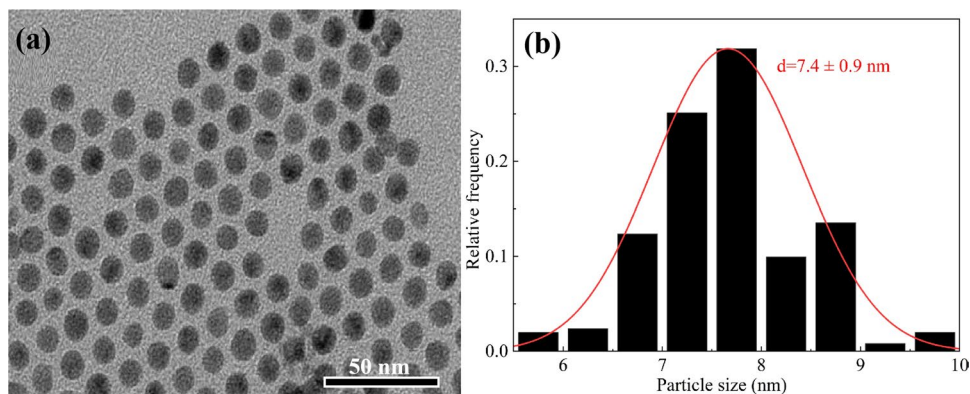
As shown in Fig. 1a, the as-synthesized PdCu nanoparticles exhibit a uniform spherical morphology. The statistical particle size distribution is displayed in Fig. 1b. It can be seen that the particle size centers in a narrow range of 6–10 nm, and the average particle size of PdCu nanoparticles is 7.4 ± 0.9 nm.

Figure 2 shows the TEM images of the synthesized Ce_{1-x}Ti_xO₂ (x = 0–0.20) and the corresponding particle size distribution. From Fig. 2 (a–e), it can be observed that all the Ce_{1-x}Ti_xO₂ samples appear in the one-dimensional rod-like shape. In order to give a deep sight into the effect of doping on the crystal growth, the average length

and width were calculated through statistical particle size distribution, as shown in Fig. 2f. The CeO₂ nanorods have an average length of 87.8 nm and a mean width of 9.4 nm. With increasing the doping amount of titanium, the length and width of the Ce_{1-x}Ti_xO₂ (x = 0–0.20) nanorods first increase and then decrease, showing a volcanic change trend. Among them, the Ce_{0.95}Ti_{0.05}O₂ nanorods have the largest length of 132 nm and width of 20 nm. However, the length and width are slightly decreased when the loading of titanium content is further increased. For the Ce_{0.9}Ti_{0.1}O₂ and Ce_{0.85}Ti_{0.15}O₂, the measured mean length and width are 119.2 nm and 16.3 nm and 91.4 nm and 13.3 nm, respectively. Except for Ce_{0.8}Ti_{0.2}O₂ nanorods, the length and width of the other Ce_{1-x}Ti_xO₂ nanorods are larger than that of pure CeO₂. Moreover, pure CeO₂ and Ce_{1-x}Ti_xO₂ with x = 0.05–0.15 appear in the uniform rod shape, while Ce_{0.8}Ti_{0.2}O₂ displays some irregular morphology. These results indicate that doping proper amount of titanium is beneficial to the grain growth of nanorods, but excessive titanium has a negative effect. In addition, the irregular morphology of Ce_{0.8}Ti_{0.2}O₂ might hint that some titanium ions do not incorporate into ceria lattices and form isolated titanium oxide.

Figure 3 shows the TEM and HRTEM images of the PdCu/Ce_{0.9}Ti_{0.1}O₂. Figure 3a displays PdCu nanoalloys which are well dispersed on Ce_{0.9}Ti_{0.1}O₂ nanorods, and no PdCu nanoalloy is found outside the rods, where some PdCu nanoalloys are circled in white. Figure 3b clearly observes the spherical PdCu nanoalloy supported on Ce_{0.9}Ti_{0.1}O₂ nanorod. The particle size of PdCu nanoalloy is about 7 nm, which is consistent with the statistical results in Fig. 1b. Also, the HRTEM image has identified the crystallographic features of the PdCu nanoalloys. The lattice fringe of 0.22 nm is attributed to the (111) plane of PdCu nanoalloy (Jiang et al. 2016). This result demonstrates that PdCu nanoalloy is formed, and these particles are well dispersed on Ce_{0.9}Ti_{0.1}O₂ nanorods by mechanical co-assembly method in this work. In addition, the rod-shaped morphology of Ce_{0.9}Ti_{0.1}O₂ remains unchanged after loading PdCu nanoalloys.

Fig. 1 (a) TEM image of PdCu active particles and (b) particle size distribution



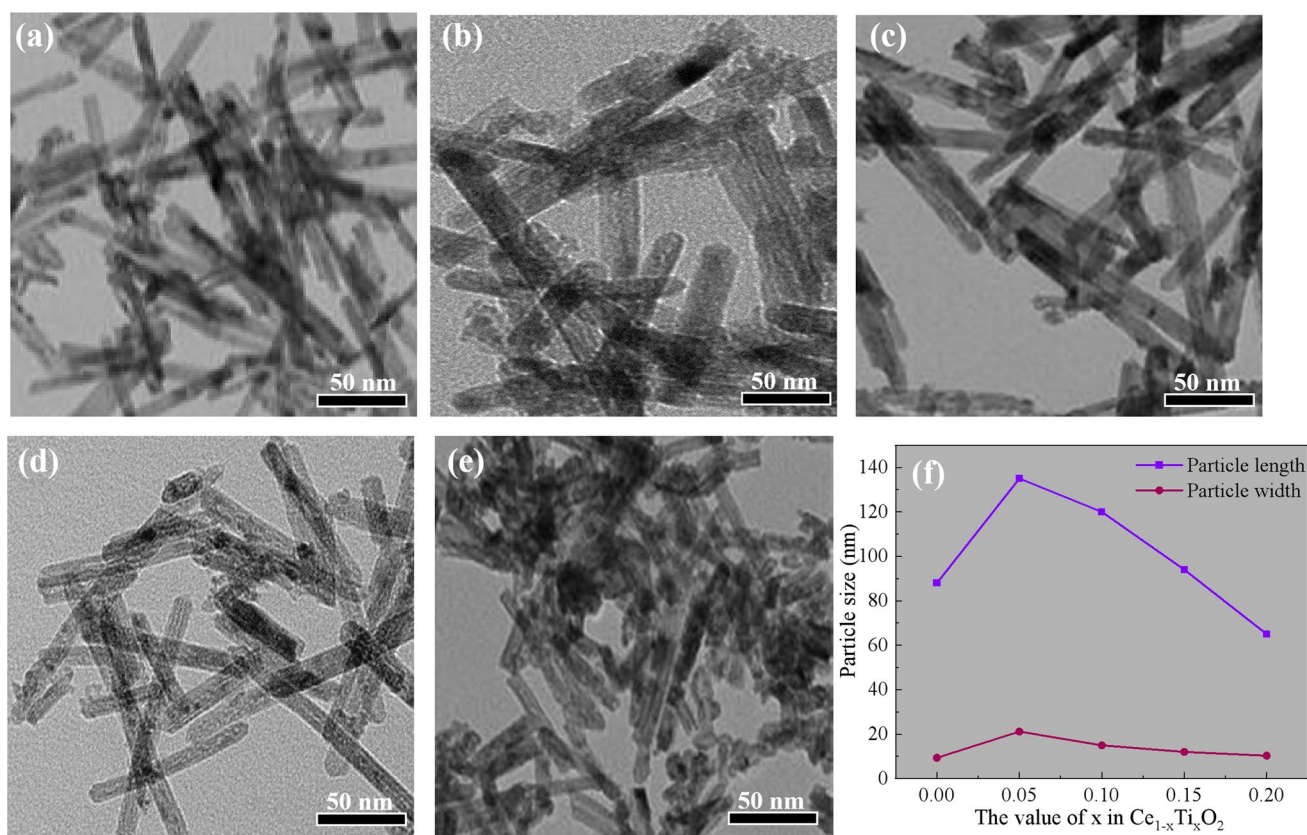
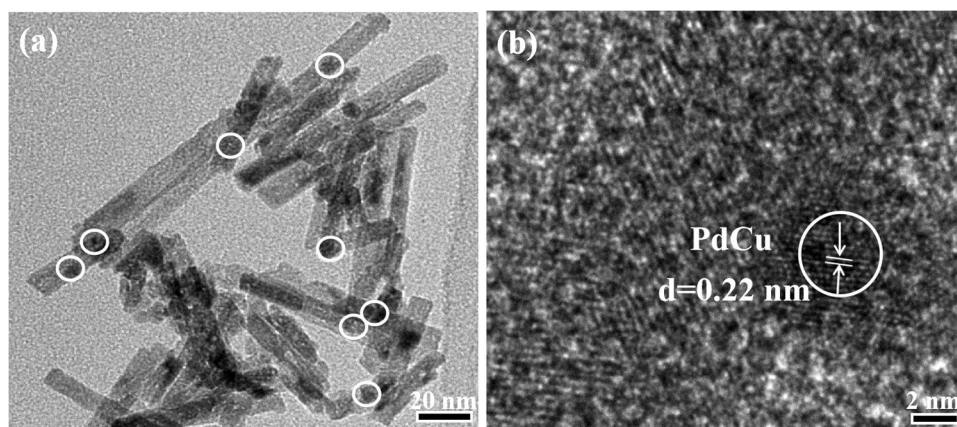


Fig. 2 TEM images of Ce_{1-x}Ti_xO₂ nanorods: (a) x=0, (b) x=0.05, (c) x=0.10, (d) x=0.15 and (e) x=0.20; (f) average length and width of Ce_{1-x}Ti_xO₂ nanorods

Fig. 3 (a) TEM and (b) HRTEM images of the PdCu/Ce_{0.9}Ti_{0.1}O₂ materials



Structural properties of samples

The crystal structure of the Ce_{1-x}Ti_xO₂ and PdCu/Ce_{1-x}Ti_xO₂ samples is measured by powder XRD. Figure 4a shows the XRD patterns of the as-synthesized Ce_{1-x}Ti_xO₂. It exhibits that these five samples all have obvious characteristic diffraction peaks, corresponding to the (111), (200), (220), (311), (222), and (400) crystal

planes of cubic fluorite CeO₂ structure. In addition, the diffraction peak of TiO₂(111) crystal plane is only observed in the Ce_{0.8}Ti_{0.2}O₂ samples. This is in accordance with the speculation from TEM results that isolated TiO₂ is formed when excessive titanium ions are added. No characteristic diffraction of TiO₂ is found for the other samples. There are two possible explanations we proposed: (1) TiO₂ incorporates into ceria lattices completely to form Ce_{1-x}Ti_xO₂

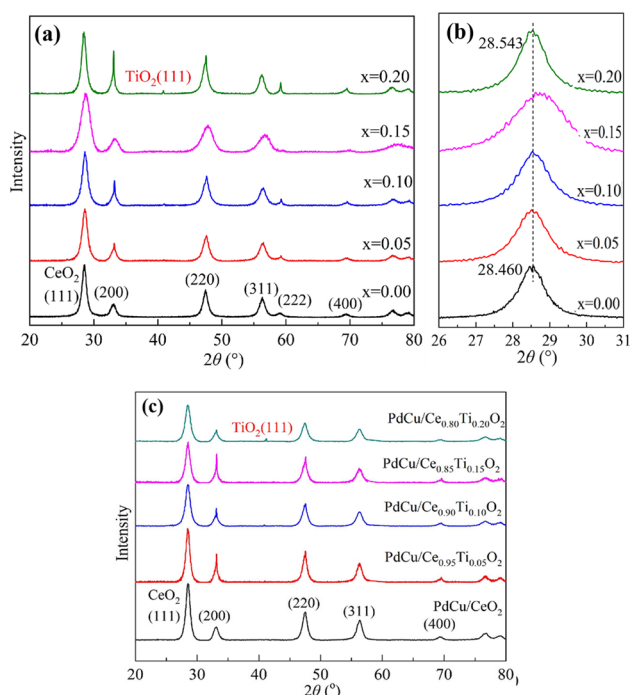


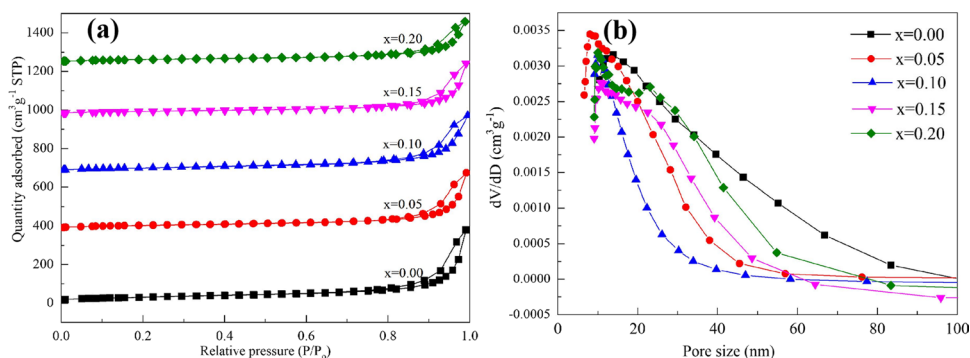
Fig. 4 (a) XRD patterns of $\text{Ce}_{1-x}\text{Ti}_x\text{O}_2$ nanorods ($x=0-0.20$) and (b) zoom in of the CeO_2 (111); (c) XRD patterns of $\text{PdCu}/\text{Ce}_{1-x}\text{Ti}_x\text{O}_2$ materials ($x=0-0.20$)

Table 1 Structural and textural properties of $\text{Ce}_{1-x}\text{Ti}_x\text{O}_2$ nanorods

Sample	(111) plane		Lattice parameter (nm)	Crystalline size (nm)
	2θ ($^\circ$)	d (nm)		
CeO_2	28.460	0.3134	0.5417	11.3
$\text{Ce}_{0.95}\text{Ti}_{0.05}\text{O}_2$	28.526	0.3127	0.5412	10.3
$\text{Ce}_{0.90}\text{Ti}_{0.10}\text{O}_2$	28.543	0.3125	0.5305	10.6
$\text{Ce}_{0.85}\text{Ti}_{0.15}\text{O}_2$	28.510	0.3128	0.5311	10.9
$\text{Ce}_{0.80}\text{Ti}_{0.20}\text{O}_2$	28.543	0.3125	0.5312	11.6

($x=0.05-0.15$) solid solution; (2) a few TiO_2 crystallites have formed, which are too small to be detected by XRD technique. It can be seen from Fig. 4b and Table 1 that

Fig. 5 (a) N_2 adsorption–desorption isotherms and (b) pore size distributions of the $\text{PdCu}/\text{Ce}_{1-x}\text{Ti}_x\text{O}_2$ materials



the (111) diffraction peak shifts to high angle after doping titanium, indicating the lattice shrinkage. This demonstrates that titanium ions have incorporated into ceria lattices, since the ionic radius of Ti^{4+} (0.072 nm) is smaller than that of Ce^{4+} (0.097 nm). The crystallite size listed in Table 1 is calculated by Scherrer's equation based on (111) diffraction. All the samples have a similar crystallite size in the range of 10.3–11.6 nm, which seems to be inconsistent with TEM results. This is because the crystallite size calculated by Scherrer's equation is the thickness perpendicular to the (111) plane.

In addition, Fig. 4c shows the XRD patterns of $\text{PdCu}/\text{Ce}_{1-x}\text{Ti}_x\text{O}_2$. Compared with Fig. 4a, no peaks related to Pd and Cu were detected. This is because the loading amount of PdCu is very low, and PdCu nanoalloys are too small and finely dispersed to be detected by XRD, as evidenced by HRTEM.

Structural and textural properties of samples

Figure 5a presents the N_2 adsorption–desorption isotherms of $\text{PdCu}/\text{Ce}_{1-x}\text{Ti}_x\text{O}_2$ catalysts. According to the IUPAC definition, all these samples exhibit the type IV isotherm, a feature of mesoporous material. The hysteresis loop of each sample is H3-type, indicating that the slit-type pores are formed in these samples as a result of nanorod accumulation. As shown in Fig. 5b, the pore size distribution of PdCu/CeO_2 centers in the range of 10–80 nm, while it firstly shrinks toward smaller diameter (10–40 nm) and then broadens towards larger diameter (10–80 nm) with increasing titanium doping amount. Accordingly, the average pore size firstly decreases and then increases as the doping amount of titanium increases, while the total pore volume exhibits the opposite tendency. The sample $\text{PdCu}/\text{Ce}_{0.9}\text{Ti}_{0.1}\text{O}_2$ has the smallest average pore size of 18.9 nm and the largest total pore volume of $0.58 \text{ cm}^3 \cdot \text{g}^{-1}$, implying that it has plentiful small pores. Particular attention should be paid to the specific surface area, which directly affects the number of active centers and reactant-catalyst contact area,

Table 2 Surface properties of PdCu/Ce_{1-x}Ti_xO₂ materials

Sample	BET surface area (m ² ·g ⁻¹)	Pore size (nm)	Pore volume (cm ³ ·g ⁻¹)
PdCu/CeO ₂	78.8	24.8	0.42
PdCu/Ce _{0.95} Ti _{0.05} O ₂	110.3	20.8	0.46
PdCu/Ce _{0.90} Ti _{0.10} O ₂	102.2	18.9	0.58
PdCu/Ce _{0.85} Ti _{0.15} O ₂	84.1	22.6	0.45
PdCu/Ce _{0.80} Ti _{0.20} O ₂	77.3	19.8	0.33

consequently the catalytic performance. As listed in Table 2, the specific surface area firstly increases and then decreases with increasing titanium doping amount, and the relatively large values of 110.3 and 102.2 m²·g⁻¹ are found for PdCu/Ce_{0.95}Ti_{0.05}O₂ and PdCu/Ce_{0.9}Ti_{0.1}O₂, respectively. The high specific surface area is expected to have a positive effect on the catalytic activity. In general, specific surface area is determined by both crystallite size and the type of grain accumulation. Since the crystallite size of PdCu/Ce_{0.95}Ti_{0.05}O₂ and PdCu/Ce_{0.9}Ti_{0.1}O₂ is relatively large, the loose accumulation of nanorods is responsible for their large specific surface area.

Chemical characteristic of samples

Doping titanium might affect the chemical state of Pd, Ce, and O, subsequently the catalytic performance. Thus the characteristic Ce 3*d*, Ti 2*p*, Pd 3*d*, and O 1*s* core levels were analyzed by XPS. Figure 6a is the XPS spectrum of Ti 2*p*_{1/2} and Ti 2*p*_{3/2}. The peaks at 457.6 eV (2*p*_{3/2}) and 463.3 eV (2*p*_{1/2}) are assigned to Ti³⁺, and the peaks at 458.8 eV and 464.5 eV are assigned to Ti⁴⁺. The different value for (Ti⁴⁺ 2*p*_{1/2} - Ti⁴⁺ 2*p*_{3/2}) and (Ti³⁺ 2*p*_{1/2} - Ti³⁺ 2*p*_{3/2}) is 5.7 eV, which is similar to the previous report (Abdullah et al. 2018). As shown in Table 3, the concentration of Ti³⁺ increases with increasing titanium content to *x* = 0.1 and then decreased with further increasing titanium content. This is also an evidence that titanium and cerium chemically interact with each other in nanorods; that is, proper amount of titanium ions is incorporated into the ceria lattice. However, excessive amount of titanium is unfavorable for the incorporation.

Figure 6b displays the Pd 3*d* XPS spectrum of the catalyst, in which four peaks corresponding to two pairs of spin orbit doublets are fitted. The binding energy of Pd 3*d*_{5/2} on the titanium-doped catalyst surface increases, which promotes the transformation of Pd to a higher oxidation state. This result indicates that the doping titanium could strengthen the metal-support interaction, and thus promote

Fig. 6 XPS spectra of PdCu/Ce_{1-x}Ti_xO₂ (*x* = 0–0.20) materials: (a) Ti 2*p*, (b) Pd 3*d*, (c) Ce 3*d*, and (d) O 1*s*

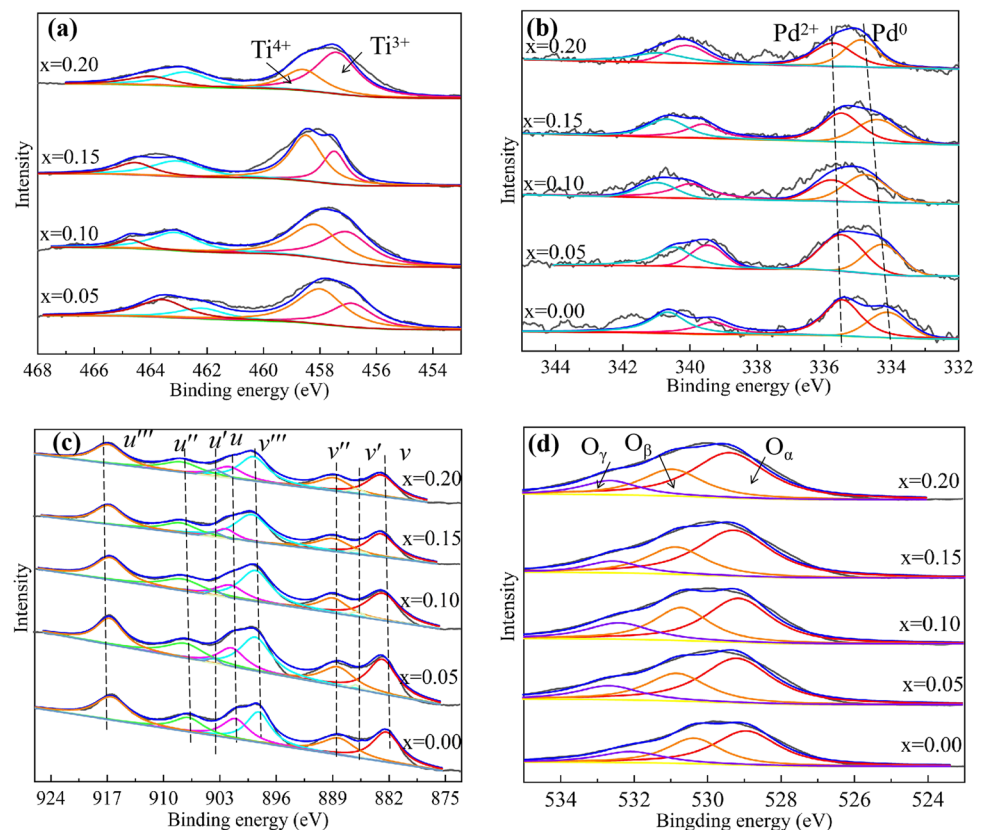


Table 3 XPS parameter of PdCu/Ce_{1-x}Ti_xO₂ materials

Samples	Surface atomic ratio (%)			
	Ti ³⁺ / (Ti ³⁺ + Ti ⁴⁺)	Pd ²⁺ /(Pd ⁰ + Pd ²⁺)	Ce ³⁺ / (Ce ³⁺ + Ce ⁴⁺)	O _β /(O _α + O _β + O _γ)
PdCu/Ce _{0.80} Ti _{0.20} O ₂	40.77	48.09	18.26	21.78
PdCu/Ce _{0.85} Ti _{0.15} O ₂	44.24	43.25	19.05	23.15
PdCu/Ce _{0.9} Ti _{0.1} O ₂	55.93	60.02	20.14	25.28
PdCu/Ce _{0.95} Ti _{0.05} O ₂	37.86	41.73	18.99	22.11
PdCu/CeO ₂	–	36.01	17.81	19.08

the electron donation from palladium to Ce_{1-x}Ti_xO₂. For the purpose of further identifying the state of palladium, we calculate the relative amount of Pd²⁺ to the total palladium; the results are shown in Table 3. It can be seen that once titanium is added, the Pd²⁺ species over the PdCu/Ce_{1-x}Ti_xO₂ increases in varying degrees compared with PdCu/CeO₂ (36.01%). Among them, the PdCu/Ce_{0.9}Ti_{0.1}O₂ sample has the highest proportion of Pd²⁺ (60.02%). Considering the largest amount of Ti³⁺ in PdCu/Ce_{0.9}Ti_{0.1}O₂, the electron transformation between palladium and titanium could be inferred. Since oxidized palladium is considered as the active species for oxidation reaction (Zhang et al. 2020), PdCu/Ce_{0.9}Ti_{0.1}O₂ may show the best catalytic activity in the complete methanol oxidation reaction.

As shown in Fig. 6c, the parallel electron spins increase the energy of the orbital energy, resulting in multiple splitting of the photoelectron peak, generating two series of spectral peaks (Ce 3d_{5/2} and Ce 3d_{3/2}). The former is marked with *v*, and the latter is marked with *u*. Where *v*, *v*"', *v*"'' and *u*, *u*"', *u*"'' are the characteristic peaks of Ce⁴⁺. And *v*' and *u*' are the characteristic peaks of Ce³⁺. According to previous reports (Wu et al. 2018), oxygen vacancies in cerium-based materials are related to the content of Ce³⁺. The higher the Ce³⁺ content is, the higher the concentration of the oxygen vacancies is. It can be seen from Table 3 that the content of Ce³⁺ is significantly increased by doping titanium ions. And the surface Ce³⁺/(Ce³⁺ + Ce⁴⁺) decreases by the following sequence: PdCu/Ce_{0.9}Ti_{0.1}O₂ > PdCu/Ce_{0.85}Ti_{0.15}O₂ > PdCu/Ce_{0.95}Ti_{0.05}O₂ > PdCu/CeO₂ > PdCu/Ce_{0.8}Ti_{0.2}O₂. This agrees well with the variation trend of the solid solution of titanium ions in ceria lattice as derived from XRD. The corresponding reason is that the lattice shrinkage induced by the insertion of Ti⁴⁺ (0.072 nm) could be alleviated by the generation of Ce³⁺ (0.103 nm). On the other hand, the variation trend of Ce³⁺/(Ce³⁺ + Ce⁴⁺) is also roughly consistent with that of Pd²⁺, because the electron donation from palladium to cerium generates Pd²⁺ and Ce³⁺. This further demonstrates that doping appropriate amount of titanium could strengthen the interaction between palladium and Ce_{1-x}Ti_xO₂ support.

Figure 6d is the XPS spectrum of O 1s. It can be seen the O 1s curves of the five catalysts are divided into three

peaks, which are centered around 529.3 eV, 530.5 eV, and 532.7 eV, respectively. The peak near 529.3 eV belongs to the lattice oxygen of the metal oxide and is denoted as O_α; the peak near 530.5 eV is denoted as O_β, which is associated with the O²⁻ ions in surface oxygen vacancies; the peak near 532.7 eV belongs to the surface oxygen from the adsorbed water and is named O_γ. The concentration of surface oxygen vacancies is estimated by the ratio of integrated peak area and the results are shown in Table 3. The O_β content of the catalyst increases by the sequence of: PdCu/Ce_{0.8}Ti_{0.2}O₂ < PdCu/CeO₂ < PdCu/Ce_{0.95}Ti_{0.05}O₂ < PdCu/Ce_{0.85}Ti_{0.15}O₂ < PdCu/Ce_{0.9}Ti_{0.1}O₂, consistent with that of Ce³⁺ content. In this regard, it is further confirmed that the insertion of titanium ions into ceria lattices favors the generation of Ce³⁺, which is paralleled with the appearance of oxygen vacancies. Previous studies have shown that the introduction of surface oxygen vacancies is beneficial to the adsorption of O₂ molecules, generating the superoxide radicals, which are considered as reactive oxygen species for oxidation reaction (Yuan et al. 2018). Considering the highest amount of surface oxygen vacancies on PdCu/Ce_{0.9}Ti_{0.1}O₂ catalyst, it might exhibit the highest activity for complete methanol oxidation. In order to verify this hypothesis, we test the catalytic performance for complete methanol oxidation, and the corresponding results are shown hereinafter.

Catalytic activity of PdCu/Ce_{1-x}Ti_xO₂ catalysts

Figure 7a shows the conversion of CH₃OH as a function of temperature over all prepared catalysts. The light-off temperature *T*₅₀ (the corresponding reaction temperature when the conversion reaches 50%) and the full conversion temperature *T*₉₀ (the corresponding reaction temperature when the conversion reaches 90%) are used as the evaluation parameters of the catalytic activity, as listed in Table 4.

As shown in Fig. 7a, for the PdCu catalysts, the introduction of titanium makes PdCu/CeO₂ much more active, and the catalytic activity first increases and then decreases as the doping amount of titanium increases. Among them, PdCu/Ce_{0.9}Ti_{0.1}O₂ shows the best catalytic activity. In detail, PdCu/Ce_{0.9}Ti_{0.1}O₂ has the *T*₅₀ of 88 °C and *T*₉₀ of 138 °C, which

Fig. 7 (a) CH₃OH conversion for PdCu/Ce_{1-x}Ti_xO₂, Pd/Ce_{0.9}Ti_{0.1}O₂ and Cu/Ce_{0.9}Ti_{0.1}O₂ catalysts; (b) stability test of PdCu/Ce_{0.9}Ti_{0.1}O₂ catalyst in 100 and 140 °C

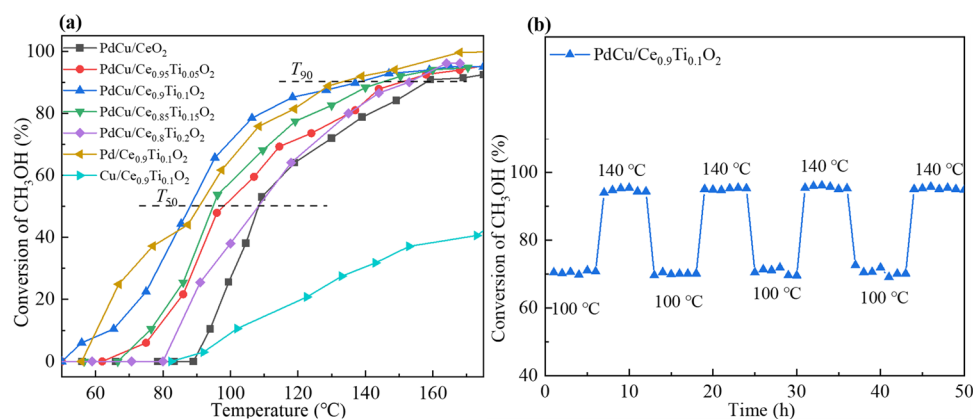


Table 4 T_{50} and T_{90} for methanol conversion on PdCu/Ce_{1-x}Ti_xO₂, Pd/Ce_{0.9}Ti_{0.1}O₂ and Cu/Ce_{0.9}Ti_{0.1}O₂ catalysts

Sample	T_{50} (°C)	T_{90} (°C)
PdCu/CeO ₂	108	159
PdCu/Ce _{0.95} Ti _{0.05} O ₂	98	152
PdCu/Ce _{0.9} Ti _{0.1} O ₂	88	138
PdCu/Ce _{0.85} Ti _{0.15} O ₂	95	145
PdCu/Ce _{0.80} Ti _{0.20} O ₂	108	153
Pd/Ce _{0.9} Ti _{0.1} O ₂	90	136
Cu/Ce _{0.9} Ti _{0.1} O ₂	185	248

are 20 °C and 21 °C lower than these of PdCu/CeO₂, respectively. With doping excessive titanium, PdCu/Ce_{0.8}Ti_{0.2}O₂ shows the worst catalytic performance, the T_{50} and T_{90} values of which are 108 °C and 153 °C, respectively. To better understand the synergistic effect between Pd and Cu in this system for CH₃OH oxidation, Pd/Ce_{0.9}Ti_{0.1}O₂ and Cu/Ce_{0.9}Ti_{0.1}O₂ (with 1 wt% Pd or Cu) catalysts are also studied. As displayed in Fig. 7a, the Cu/Ce_{0.9}Ti_{0.1}O₂ catalyst shows very poor catalytic activity of CH₃OH oxidation. When the temperature increases to 170 °C, the conversion of CH₃OH is still less than 50%. Besides, as summarized in Table 4, the light-off temperature and full conversion temperature of CH₃OH of Pd/Ce_{0.9}Ti_{0.1}O₂ and PdCu/Ce_{0.9}Ti_{0.1}O₂ are nearly identical, and T_{50} and T_{90} are about 90 °C and 138 °C, respectively. However, PdCu/Ce_{0.9}Ti_{0.1}O₂ is considered to be better because its Pd loading (0.75 wt%) is less than that of Pd/Ce_{0.9}Ti_{0.1}O₂ (1 wt%). Combined with above characterizations, three possible reasons for the best catalytic of PdCu/Ce_{0.9}Ti_{0.1}O₂ are given as follows: (1) PdCu/Ce_{0.9}Ti_{0.1}O₂ possesses the relatively large surface area and the largest pore value, which magnifies the reactant-catalyst contact area and promotes the mass transfer process; (2) the largest amount of surface oxygen vacancies on PdCu/Ce_{0.9}Ti_{0.1}O₂ is beneficial to the chemisorption and activation of oxygen molecules; (3) PdCu/Ce_{0.9}Ti_{0.1}O₂ has the highest proportion of Pd²⁺ that is considered as the reactive sites for methanol

oxidation, which is the primary reason for its excellent activity. Finally, the PdCu/Ce_{0.9}Ti_{0.1}O₂ is chosen for evaluating its catalytic stability and repeatability during CH₃OH oxidation reaction at different conversions. As shown in Fig. 7b, the PdCu/Ce_{0.9}Ti_{0.1}O₂ exhibits remarkable stability and excellent repeatability in the whole test period. Meanwhile, no by-products are observed throughout the process of catalytic activity, stability and repeatability.

Conclusions

In this work, we prepared a high-activity and stability PdCu/Ce_{1-x}Ti_xO₂ ($x=0-0.20$) catalyst for complete methanol oxidation, and studied the influence of the titanium doping content on this catalyst. Combined with multiple characterizations, it is confirmed that the metal-support interaction is greatly enhanced with the introduction of titanium, inducing electron transfer between Ce_{1-x}Ti_xO₂ and PdCu, which subsequently promotes to produce more oxidized palladium species and surface oxygen vacancies on the catalyst, but excessive titanium has a negative effect. Among the five catalysts, the PdCu/Ce_{0.9}Ti_{0.1}O₂ catalyst has the largest amount of oxidized palladium species and surface oxygen vacancies. Consequently, the PdCu/Ce_{0.9}Ti_{0.1}O₂ catalyst has the highest catalytic activity, over which the T_{50} and T_{90} of methanol oxidation are 88 °C and 138 °C, respectively. Except PdCu/Ce_{0.8}Ti_{0.2}O₂, the metal-support interaction is strengthened to a certain extent by doping titanium, thus these modified PdCu/Ce_{1-x}Ti_xO₂ catalysts show a better catalytic activity than the unmodified one. In addition, no by-products are observed during the catalytic process and no significant decrease in catalytic activity after long-term use. This work verifies the promising potential of PdCu/Ce_{1-x}Ti_xO₂ catalysts for purifying automobile exhaust.

Author contribution Zhangjie Li: writing—original draft preparation; data curation; catalyst activity tests.

Yongdong Chen: writing—reviewing and editing.
 Jie Deng: writing—reviewing and editing.
 Li Luo: writing—reviewing and editing.
 Wenxiang Gao: writing—reviewing and editing.
 Liang Yuan: writing—reviewing and editing.

Funding This work was supported by the National Natural Science Foundation of China (No. 21773189), the Project of Department of Science and Technology of Sichuan Province (No. 19ZDZX0113), the Central Government Funds of Guiding Local Scientific and Technological Development for Sichuan Province (No. 2021ZYD0044) and the Science Research Starting Project of SWPU (No. 2021QHZ023).

Data availability We declare that all the data supporting the results of this paper were generated during this study.

Declarations

Ethics approval and consent to participate Not applicable.

Consent for publication Not applicable.

Competing interests The authors declare no competing interests.

References

- Aakko-Saksa P, Koponen P, Roslund P, Laurikko J, Nylund N-O, Karjalainen P, Rönkkö T, Timonen H (2020) Comprehensive emission characterisation of exhaust from alternative fuelled car. *Atmos Environ* 236:117643
- Abdullah SA, Sahdan MZ, Nafarizal N, Saim H, Embong Z, Rohaida CHC, Adriyanto F (2018) Influence of substrate annealing on inducing Ti³⁺ and oxygen vacancy in TiO₂ thin films deposited via RF magnetron sputtering. *Appl Surf Sci* 462:575–582. <https://doi.org/10.1016/j.apsusc.2018.08.137>
- Antonia IM, Andrea V, Aldo T, Mojtaba GK, Alessandro G, Raffaello M, Vittorio M, Alberto V, Elisa M (2020) Au-decorated Ce-Ti mixed oxides for efficient CO preferential photooxidation. *ACS Appl Mater Interfaces* 34:38019–38030
- Arnason B, Sigfússon T (1999) Converting CO₂ emissions and hydrogen into methanol vehicle fuel. *Jom* 51:46–47
- Chen D, He D, Lu J, Zhong L, Liu F, Liu J, Yu J, Wan G, He S, Luo Y (2017) Investigation of the role of surface lattice oxygen and bulk lattice oxygen migration of cerium-based oxygen carriers: XPS and designed H₂-TPR characterization. *Applied Catalysis B* 218:249–259
- Chen Z, He Y, Chen J, Fu X, Sun R, Chen Y, Wong C (2018) PdCu alloy flower-like nanocages with high electrocatalytic performance for methanol oxidation. *J Phys Chem C* 16:8976–8983
- Chen W, Yu Z, Zhu Z (2019a) Effects of cerium oxides on the catalytic performance of Pd/CNT for methanol oxidation. *Chem Res Chin Univ* 35:133–138
- Chen Y, Wang H, Qin Z, Tian S, Li G (2019b) Ti_xCe_{1-x}O₂ nanocomposites: a monolithic catalyst for the direct conversion of carbon dioxide and methanol to dimethyl carbonate. *Green Chem* 21:4642–4649
- Cui S, Li R, Zhu C, Pie J, Wen Y (2020) Cerium-bismuth solid solution material prepared and application in automobile exhaust purification. *Sep Purif Technol* 239:116520
- Gholinejad M, Khosravi F, Afrasi M, Sansano JM, Nájera C (2021) Applications of bimetallic PdCu catalysts. *Catal Sci Technol* 11:2652–2702
- Grieshammer S (2017) Defect interactions in the CeO₂-ZrO₂-Y₂O₃ solid solution. *J Phys Chem C* 121:15078–15084
- Guo Z, Kang X, Zheng X, Huang J, Chen S (2019) PdCu alloy nanoparticles supported on CeO₂ nanorods: enhanced electrocatalytic activity by synergy of compressive strain, PdO and oxygen vacancy. *J Catal* 374:101–109
- Hao Z, Shen J, Lin S, Han X, Chang X, Liu J, Li M, Ma X (2021) Decoupling the effect of Ni particle size and surface oxygen deficiencies in CO₂ methanation over ceria supported Ni. *Appl Catal B* 286:1–10
- Jiang K, Wang P, Guo S, Zhang X, Shen X, Lu G, Su D, Huang X (2016) Ordered PdCu-based nanoparticles as bifunctional oxygen-reduction and ethanol-oxidation electrocatalysts. *Angew Chem* 55:9030–9035
- Kumar S, Mahajan M, Singh R, Mahajan A (2018) Silver nanoparticles anchored reduced graphene oxide for enhanced electrocatalytic activity towards methanol oxidation. *Chem Phys Lett* 693:23–27
- Li L, Zhao S, Zhou Z, Liu J (2021) Determination of unburned methanol in methanol automobile exhaust. *Automob Appl Technol*. pp 151–154
- Li W, Wey M (2021) Dual immobilization of Pd single bond Cu nanoparticles on halloysite nanotubes by CTAB and PVP for automobile exhaust elimination. *Appl Clay Sci* 214:1–10
- Luo Y, Xiao Y, Cai G, Zheng Y, Wei K (2012) A study of barium doped Pd/Al₂O₃-Ce_{0.3}Zr_{0.7}O₂ catalyst for complete methanol oxidation. *Catal Commun* 27:134–137
- Luo Y, Qian Q, Chen Q (2015) On the promoting effect of the addition of Ce_xZr_{1-x}O₂ to palladium based alumina catalysts for methanol deep oxidation. *Mater Res Bull* 62:65–70
- Manzorro R, Pérez-Omil JA, Calvino JJ, Trasobares S (2019) Understanding the complex structure of CeO₂/TiO₂ nanocatalyst. Key contributions of the combined use of HAADF, X-EDS and EELS spectroscopies. *Microsc Microanal* 25:578–579
- Satra J, Ghorui UK, Mondal P, Bhadu GR, Adhikary B (2020) One pot solvent assisted syntheses of Ag₃SbS₃ nanocrystals and exploring their phase dependent electrochemical behavior toward oxygen reduction reaction and visible light induced methanol oxidation reaction. *Dalton Trans* 49:9464–9479
- Shan Y, Liu Y, Li Y, Yang W (2020) A review on application of cerium-based oxides in gaseous pollutant purification. *Sep Purif Technol* 250:117181
- Su S, Ge Y, Wang X, Zhang M, Hao L, Tan J, Shi F, Guo D, Yang Z (2020) Evaluating the in-service emissions of high-mileage dedicated methanol-fueled passenger cars: regulated and unregulated emissions. *Energies* 13:2680
- Tang X, Wang X, Yang L, Zhang Z, Wang J, Luo J (2020) Multifunctional nickel nanofiber for effective air purification: PM removal and NO reduction from automobile exhaust. *J Mater Sci* 55:6161–6171
- Tian X, Wang L, Deng P, Yu C, Xia B (2017) Research advances in unsupported Pt-based catalysts for electrochemical methanol oxidation. *J Energy Chem* 26:1067–1076
- Tian H, Yu Y, Wang Q, Li P, Rao P, Li R, Du Y, Jia C, Luo J, Deng P, Shen Y, Tian X (2021) Recent advances in two-dimensional Pt based electrocatalysts for methanol oxidation reaction. *Int J Hydrog Energy* 46:31202–31215
- Wang L, Li Y, Liu J, Tian Z, Jing Y (2021a) Regulation of oxygen vacancies in cobalt-cerium oxide catalyst for boosting decontamination of VOCs by catalytic oxidation. *Sep Purif Technol* 277:119505

- Wang L, Yu X, Wei Y, Liu J, Zhao Z (2021b) Research advances of rare earth catalysts for the catalytic purification of vehicle exhausts. *J Rare Earths* 39:1151–1180
- Wu JM, Xing H (2020) Facet-dependent decoration of TiO₂ mesocrystals on TiO₂ microcrystals for enhanced photoactivity. *Nanotechnology* 31:1–8
- Wu W, Savereide LM, Notestein J, Weitz E (2018) In-situ IR spectroscopy as a probe of oxidation/reduction of Ce in nanostructured CeO₂. *Appl Surf Sci* 445:548–554
- Yuan H, Li J, Yang W, Zhuang Z, Zhao Y, He L, Xu L, Liao X, Zhu R, Mai L (2018) Oxygen vacancy-determined highly efficient oxygen reduction in NiCo₂O₄/hollow carbon spheres. *ACS Appl Mater Interfaces* 10:16410–16417
- Zhang G, Zhang G, Han W, Han W, Dong F, Dong F, Zong L, Zong L, Lu G, Lu G (2016) One pot synthesis of a highly efficient mesoporous ceria-titanium catalyst for selective catalytic reduction of NO. *RSC Adv* 6:76556–76567
- Zhang X, Chen X, Liu Y, Guo M (2020) Effects of support on performance of methanol oxidation over palladium-only catalysts. *Water Air Soil Pollut* 231:1–12
- Zhen X, Liu D, Wang Y (2017) The knock study of methanol fuel based on multi-dimensional simulation analysis. *Energy* 122:552–559

Publisher's note Springer Nature remains neutral with regard to jurisdictional claims in published maps and institutional affiliations.